Journal of Environmental Chemical Engineering 13 (2025) 118515

Contents lists available at ScienceDirect

Journal of Environmental Chemical Engineering

journal homepage: www.elsevier.com/locate/jece

Roles of dissolved organic matters in K-struvite formation in batch and fluidized-bed reactors: A kinetic insight

Muhammad Bilal Zahid [a], Xianfei Wang [a], Yangfan Xia [a], Xinyi Xu [b], Dawei Li [a], Feihu Li [a,b,*]

[a] Collaborative Innovation Center of Atmospheric Environment and Equipment Technology, Jiangsu Key Laboratory of Atmospheric Environment Monitoring and Pollution Control, School of Environmental Science and Engineering, Nanjing University of Information Science and Technology, 219 Ningliu Road, Nanjing 210044, China

[b] NUIST Reading Academy, Nanjing University of Information Science and Technology, 219 Ningliu Road, Nanjing 210044, China

ARTICLE INFO

Keywords:
K-struvite
Dissolved organic matter
Fluidized-bed reactor
Phosphorus recovery
Wastewater treatment

ABSTRACT

Struvite crystallization is a widely used technique for reclaiming nitrogen and phosphorus from waste streams. K-struvite, an analogue of struvite (NH_4^+), has attracted ever-growing attention as its precipitation often occurs under conditions similar to struvite (thereby, reactions can be implemented in existing facilities). However, K-struvite formation is usually influenced by co-occurring impurities, particularly dissolved organic matters (DOMs). Here, we evaluated the roles of three typical DOMs (i.e., L-arginine, citric acid, and humic acid) in K-struvite crystallization from a reaction kinetic perspective. It was found that K-struvite crystallization follows a well-defined first-order kinetics in the absence of any DOMs, regardless of the Mg/P molar ratio and supersaturation level. The presence of DOMs at varying levels (2 −50 mg L^{-1}) has been shown to have strong inhibition against K-struvite formation in batch reactors, with L-arginine acting as a phosphate binder, citric and humic acids as chelators of magnesium and potassium ions, and all DOMs as crystallization passivators via surface adsorption. Crystallographic and morphological analyses reveal that a lower supersaturation (0.47) level tends to yield amorphous precipitates with a small fraction of poorly crystallized K-struvite, failing to compensate for the inhibition from DOMs. While both the kinetic modeling and the structural examination indicate that the DOM inhibition was suppressed at a supersaturation as high as 2.57. In fluidized-bed reactors with a feed solution of a higher supersaturation (2.53), the natural DOMs appear to alter the phase composition and morphology significantly, with a majority of amorphous aggregates along with a few hexagonal K-struvite and shuttle-like vivianite crystals. Electrostatic potential mapping analysis of these DOMs reveals that the inhibition mechanisms varied with the type of DOMs, and future work would be necessary for molecular-level elucidation of the DOM-specific inhibition. This study offers a kinetic insight into K-struvite formation and underscores the necessity of strategies to tackle DOM-related issues in practical projects.

1. Introduction

Phosphorus (P) is a vital component of all known life forms and essential to cellular processes on Earth—yet its future is precarious [1,2]. Projections of the ever-growing depletion of global phosphorus reserves in this century raise significant concerns about food security and ecological stability [3,4]. The ubiquity of phosphorus compounds—from agricultural fertilizers to water-softening agents in household detergents—underscores its indispensable role in sustaining human activities [5]. However, its increasing consumption presents an environmental paradox: excessive phosphorus entering aquatic ecosystems drives eutrophication [2,5]. Historically, wastewater treatment strategies have focused on complete phosphate removal to minimize environmental harm from nutrient pollution [6,7]. While effective in mitigating eutrophication, this approach overlooks the vast potential for phosphorus recovery and reuse, treating it as a waste product rather than a valuable resource [5,8]. Nevertheless, wastewater represents a readily available source of phosphate. Given the rising global demand for phosphorus, recovering and reclaiming phosphorus from wastewater is gaining increasing attention [9–11].

* Corresponding author at: Collaborative Innovation Center of Atmospheric Environment and Equipment Technology, Jiangsu Key Laboratory of Atmospheric Environment Monitoring and Pollution Control, School of Environmental Science and Engineering, Nanjing University of Information Science and Technology, 219 Ningliu Road, Nanjing 210044, China.
E-mail address: fhli@nuist.edu.cn (F. Li).

https://doi.org/10.1016/j.jece.2025.118515
Received 21 June 2025; Received in revised form 3 August 2025; Accepted 5 August 2025
Available online 6 August 2025

To date, various chemical, biological, and physical processes [6,9], along with advanced crystallization technologies [11,12], have been employed for phosphorus recovery from wastewater. Among these, fluidized-bed crystallization (FBC) has emerged as a promising chemical method due to its ability to process large solution volumes and precisely control crystal size [10]. Initially developed for water-softening granulation, FBC technology has evolved from early experimental stages to large-scale industrial applications [8,10,11]. Generally, struvite ($MgNH_4PO_4{\cdot}6H_2O$, also known as magnesium ammonium phosphate, MAP) is the predominant crystalline product recovered through FBC technology and is widely regarded as a promising recycled fertilizer due to its high phosphorus content and slow-release properties [12–14]. However, in wastewaters where potassium (K^+) dominates over ammonium (NH_4^+), K-struvite ($KMgPO_4{\cdot}6H_2O$, all termed as potassium magnesium phosphate, MKP) can form as an alternative phosphate mineral, incorporating potassium into its crystalline structure [15,16]. This analogue retains similar fertilizing benefits while adapting to the ionic composition of the wastewater stream [16].

Notably, the formation kinetics, morphology, purity, and overall quality of the resulting struvite are usually influenced by the co-occurring impurities [17–23], particularly the dissolved organic matters (DOMs) [18–23], which is a heterogeneous mixture of organic compounds ubiquitously present in wastewater, primarily originating from humic substances, proteins, polysaccharides, and microbial byproducts [19,21,24]. These compounds vary in molecular weight, functional groups (e.g., carboxyl, hydroxyl, and amine groups), and hydrophobicity, influencing their reactivity in aqueous environments [19,22,24,25]. In P recovery systems, DOMs can significantly alter crystallization processes due to their ability to interact with inorganic ions and crystal surfaces [18–23]. For instance, humic acids—a major DOM component—can adsorb onto growing struvite crystals, blocking active growth sites and impeding crystal development through surface passivation [26,27]. Similarly, low-molecular-weight organic acids (e.g., citrates) may chelate magnesium (Mg^{2+}) or phosphate (PO_4^{3-}) ions in solution, reducing their bioavailability for crystallization [28,29]. These interactions can lead to slower nucleation rates, smaller crystal sizes, or even amorphous precipitate formation, ultimately affecting the efficiency and quality of recovered products. While previous studies have extensively explored DOM's inhibitory effects on conventional struvite formation, their impact on K-struvite—an analogue of struvite [30]—remains poorly understood [31,32]. Furthermore, the roles of DOM in altering the morphology, purity, and settling properties of K-struvite—key factors in its suitability as a fertilizer—have yet to be systematically investigated. Addressing these unknowns is essential for optimizing reactor design and operational parameters to achieve consistent recovery performance in DOM-rich waste streams, such as agro-industrial effluents or anaerobically digested sludge liquors. Bridging this knowledge gap would not only advance a fundamental understanding of organic-inorganic interactions in crystallization processes but also support the scalable application of K-struvite recovery technologies in real-world wastewater treatment systems.

This study presents a systematic investigation of how DOM governs the crystallization kinetics of K-struvite formation across different reactor configurations, aiming to elucidate the fundamental roles of DOM in influencing K-struvite crystallization dynamics. Given the DOM-type impurities in actual wastewater are complex and of concentrations spanning a broad range of several to thousands of mg L^{-1} [33–35], simulated DOMs (e.g., humic acid (HA), L-arginine (Arg), and citric acid (CA)) are often used as surrogates to represent the reactive fraction of such organic matters [24,27,33,36]. We specifically examine three representative organic constituents of wastewater, i.e., Arg, CA, and HA, to elucidate their distinct impacts on nucleation and crystal growth inhibition in both batch reactor (BR) and fluidized-bed reactor (FBR) systems. Through controlled batch kinetic experiments, we demonstrate how increasing DOM concentrations fundamentally alter crystallization dynamics. Parallel FBR studies reveal how natural DOMs modulate these organic-inorganic interactions, offering new insights into K-struvite crystallization behavior. Beyond advancing a fundamental understanding of K-struvite crystallization in the presence of DOMs, this research also offers practical implications for wastewater treatment optimization, enabling informed reactor selection and operational parameter tuning for enhanced nutrient recovery efficiency.

2. Materials and methods

2.1. Chemicals

Chemicals of analytical purity or above were used for K-struvite crystallization in this study. Monopotassium phosphate (KH_2PO_4, ≥99.0 %), magnesium chloride hexahydrate ($MgCl_2{\cdot}6H_2O$, ≥98.0 %), and sodium hydroxide (NaOH, ≥99.0 %) were purchased from Sinopharm Chemical Reagent Co., Ltd (Shanghai, China). L-arginine (Arg, $C_6H_{14}N_4O_2$), citric acid (CA, $C_6H_8O_7{\cdot}H_2O$), and humic acid (HA) were provided by Yuanye Bio-Technology Co., Ltd (Shanghai, China). Ultrapure deionized (DI) water (18.2 MΩ·cm, 25 °C) was employed for preparing solutions.

2.2. K-struvite crystallization in batch reactors (BRs)

Batch crystallization kinetic experiments (Scheme 1) were conducted with a varying Mg/P molar ratio using a 1000-mL glass beaker as the batch reactor (Fig. S1, Supporting Information) under ambitious conditions (*ca.* 25 °C, 1 atm). Prior studies have shown that K-struvite crystallization is most sensitive to Mg/P molar ratio, with K^+ equal to or above stoichiometry does not markedly affect removal efficacy or product purity [31,37,38]. Therefore, Mg/P molar ratios of 1.2 −1.5:1 were examined comprehensively. In brief, solution A was prepared by dissolving 0.2106 mmol KH_2PO_4 into 500 mL of DI water, and then a diluted NaOH solution was added until the pH reached 10 ± 0.2. Likewise, solution B was prepared by mixing 0.2106 mmol of $MgCl_2{\cdot}6H_2O$ into 500 mL of DI water, followed by rapidly transferring it to the above beaker, yielding a mixture containing 0.2106 mM of Mg^{2+}, K^+, and PO_4^{3-} in a 1:1:1 molar ratio. The mixture with a supersaturation index (SI, Text S1, Supporting Information) of 0.47 was then stirred moderately on a magnetic stirrer (INTLLAB, Shenzhen, China). The pH of the synthetic mixture was monitored and recorded every 2 min using a pH meter (PHS-25, Rex Electric Chemical, China) for 60 min, while 0.1 mL of suspension was sampled every 2 min to measure the concentration of remaining soluble phosphate (PO_4^{3-}-P) using the ascorbic acid method as described elsewhere [39]. Following the same protocol, Arg, CA, and HA were used as the model DOM-type impurities for examining their impact on the crystallization of K-struvite at a constant Mg/P molar ratio of 1:1. Specifically, each impurity was introduced separately into the mixture when combining solutions A and B. Prior studies have documented that

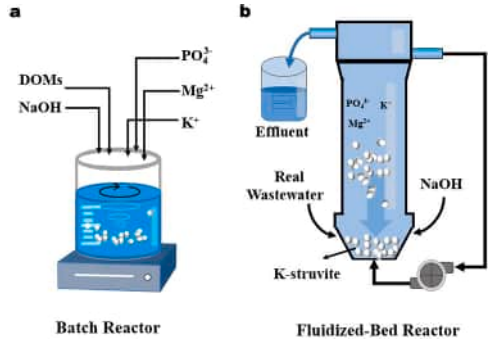

Scheme 1. Schematic view of (**a**) batch reactor (BR), and (**b**) fluidized bed reactor (FBR) for K-struvite crystallization.

the DOM concentrations span a wide range, with values in the order of several to tens of mg L^{-1} dissolved organic carbon (DOC) (e.g., 5 −50 mg L^{-1}) in municipal wastewater streams and/or treated effluents [34–36]. To representatively simulate the typical municipal wastewater streams, we chosed experimental DOM concentration window of 2–50 ppm [20], which is rational given that the COD values obtained with the typical oxidation factor (i.e., 2.67) [40] and the maximum DOM concentration (50 mg L^{-1}) are comparable to the actual wastewater COD values (Table S1). The resulting suspension was termed based on the type and content of impurity in the mixture, e.g., Arg-2ppm refers to a suspension containing 2 mg L^{-1} of Arg. After each round of batch reaction (i.e., 60 min), all the precipitate samples were collected by centrifugation, rinsed twice with DI water, and dried in an oven at 80 °C overnight. The precipitates were allowed to cool to ambient temperature in a glass desiccator, denoted by the same code as their parent suspensions, and left in the desiccator for later characterization.

The rate constant for crystallization kinetics was obtained by fitting the data of remaining soluble phosphate in the suspensions to a first-order kinetic model as described in differential and linear forms of the model formulated in Eqs. 1 and 2, respectively [41].

$$-dC/dt = k(C_0 - C_e) \quad (1)$$

$$\ln(C - C_e) = -kb + \ln(C_O - C_e) \quad (2)$$

where k is the rate constant (h^{-1}), C is the soluble phosphate (reactant) concentration (mg L^{-1}) at time t, C_0 and C_e are the phosphate (PO_4^{3-}-P) concentration at the initial and equilibrium state (mmol L^{-1}).

2.3. K-struvite crystallization in a fluidized-bed reactor (FBR)

A customer-made FBR was used to evaluate the influence of natural DOM molecules from real wastewater on K-struvite formation (Fig. S2, Supporting Information). The FBR feed solution (~5 L) was composed of real wastewater from a local sewage treatment plant (Table S1), whose Mg/P and PO_4^{3-} concentration were adjusted to 1:1 and 150 mg L^{-1}, respectively, by adding appropriate quantities of $MgCl_2{\cdot}6H_2O$ and KH_2PO_4. NaOH solution (0.1 M) was added to adjust the initial pH of the feed solution above 10 during the FBR operation. Firstly, the feed solution was injected into the FBR at a flow rate of 5 mL min^{-1} by using a peristaltic pump (BT-100, Longer Pump Co., China). Then, the NaOH solution was introduced at 3 mL min^{-1} using another pump, and the third pump connecting the bottom and the upper top of the FBR was launched simultaneously at 10 mL min^{-1} to circulate the mixture and maintain a fluidization condition. At the end of the 6-day circulation, the experiment was terminated, and the precipitates were harvested from the FBR bottom (Fig. S2), followed by centrifugal separation, washing, and air drying over 24 h before characterization.

2.4. Characterization of the reclaimed precipitates

X-ray diffraction (XRD) measurements were carried out using an XRD-6100 diffractor (Shimadzu, Japan) system with Cu-K radiation (λ = 1.54178 Å) over the 2θ range of 10 – 60°. The identification of all mineral phases was carried out using the Jade software (version 9.0, Materials Data Inc., USA) with the ICDD® PDF-2 database. Fourier transform infrared (FTIR) spectroscopy was recorded on a Nicolet iS5 spectrometer (Thermo Fisher, USA) using the KBr pellet method in the wave number range of 4000 – 400 cm^{-1}. The morphology of reclaimed precipitates was examined using a Gemini 300 field emission scanning electron microscope (FE-SEM, ZEISS, Germany) at an acceleration voltage of 15 kV.

3. Results and discussion

3.1. Effects of Mg/P molar ratio on K-struvite formation kinetics in BRs

The influence of the Mg/P molar ratio on K-struvite crystallization in batch reactors is multifactorial, driven mainly by the molar ratios of the participating species and the extent of supersaturation [42]. For the precipitation of pure K-struvite in batch reactors, the optimal molar ratio of Mg/P is important, particularly for the exploration of the impact of other impurities. Batch reaction experiments were performed to evaluate the effects of Mg/P molar ratios (i.e., 1:1, 1.2:1, and 1.5:1) on the removal of PO_4^{3-}, and thereof K-struvite formation kinetics indirectly (Fig. 1). As shown in Fig. 1a, the solution pH decreased apparently with time in all studied Mg/P molar ratios, with faster and much more pH drops at higher Mg/P ratios. This phenomenon can be explained based on the following two reactions (Eq.3 and Eq. 4):

i) The formation of $MgKPO_4{\cdot}6H_2O$:

$$Mg^{2+} + K^+ + HPO_4^{2-} + 6H_2O \rightarrow MgKPO_4{\bullet}6H_2O\downarrow + H^+ \quad (3)$$

ii) The hydrolysis of free Mg^{2+}:

$$Mg^{2+} + 2H_2O \rightleftharpoons Mg(OH)^+ + H_3O^+ \quad (4)$$

Both reactions release hydrogen (or hydronium, H_3O^+) ions, directly increasing the solution's acidity. At higher Mg/P ratios, excess Mg^{2+} drives the K-struvite formation reaction (Eq. 3) further to completion [43], consuming more HPO_4^{2-} and releasing more H^+. Besides, the remaining free Mg^{2+} (not precipitated) undergoes hydrolysis in water (Eq. 4), further lowering pH by releasing additional hydronium ions. This is further confirmed by the soluble phosphate concentrations (PO_4^{3-}-P) versus time plots (Fig. 1b), showcasing lower free PO_4^{3-}-P concentrations at higher Mg/P ratios. Note that the removal of PO_4^{3-} at Mg/P ratio of 1:1 reached as much as 98 % at 55 min, while P removal for Mg/P ratios of 1.2:1 and 1.5:1 at the same time was determined as 99 %, with a maximum of ~ 99.3 % for all three Mg/P ratios at the end of the batch reactions (Fig. 1b). This observation implies 60 min is enough to implement the complete crystallization of K-struvite irrespective of the Mg/P ratio. Prior studies [44] have shown that excess magnesium (high Mg/P) not only increases supersaturation but also promotes secondary nucleation of K-struvite on intermediate phases such as $Mg(OH)_2$, which can facilitate heterogeneous nucleation of K-struvite [45]. To verify this possible pathway of K-struvite formation promoted by $Mg(OH)_2$, the precipitates from solutions with Mg/P ratios of 1.2 and 1.5 were reclaimed and examined by XRD and FTIR (Fig. S3). Our results confirmed the absence of $Mg(OH)_2$ in the reclaimed precipitates that are mainly composed of poorly crystalline K-struvite (PDF #35–0812), thus excluding such 'Mg(OH)$_2$-mediated' mechanism.

The remaining phosphate concentration as a function of time was then further fitted using a first-order kinetic model (Eq. 2), and the results are depicted in Fig. 1c-e. All plots are linear with negative slopes as expected. Notably, all the best-fit correlation coefficients (R^2) are greater than 0.98 (Table 1), indicating the formation of K-struvite in BRs follows a well-defined first-order kinetics within the time scale of 0 −14 min, regardless of the Mg/P ratios. The highest rate constant (k) is 5.4834 h^{-1} for suspension with a Mg/P ratio of 1.5:1, further confirming that higher Mg/P ratios accelerate K-struvite crystallization, namely higher Mg/P ratios boost faster crystallization kinetics. However, it was found that K-struvite crystallization may be inhibited a little bit at much higher Mg/P ratios [46]. With elevated Mg/P ratios beyond 2.0, for instance, the K-struvite crystallization is significantly inhibited due to the precipitation of $Mg_3(PO_4)_2{\cdot}22H_2O$ and $Mg_3(PO_4)_2{\cdot}8H_2O$ [47,48]. To avoid such uncertainty for preparing pure K-struvite, an optimal stoichiometric Mg/P ratio of 1:1 was therefore chosen for the following batch experiments.

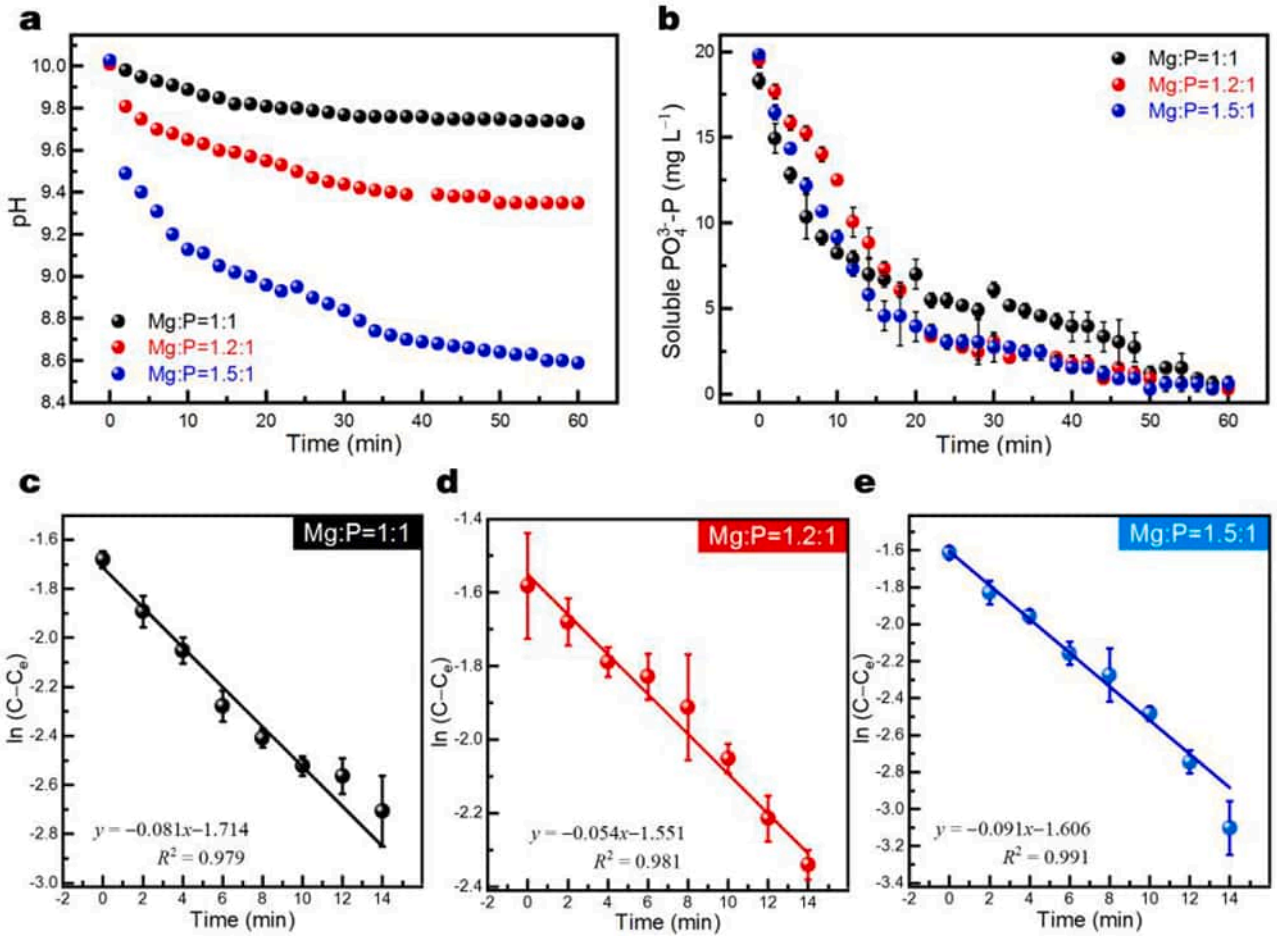

Fig. 1. (**a**) The suspension pH profiles in solutions with 0.028 mM of PO_4^{3-}-P, (**b**) Plots of soluble PO_4^{3-}-P versus reaction time, (**c**) Kinetic linear fitting plots of soluble PO_4^{3-}-P in suspensions with Mg/P ratio of (**c**) 1:1 (**d**) 1.2:1 and **(e)** 1.5:1 during the K-struvite crystallization in batch reactors.

Table 1
Best-fit kinetic equations and corresponding parameters of K-struvite formation in BRs with varying Mg/P ratio based on the first-order kinetic model.

Mg/P ratio	First-order kinetic equation	k (h^{-1})	Time scale (min)	R^2
1:1	$y = -0.081x - 1.714$	4.312 ± 0.317	0–14	0.979
1.2:1	$y = -0.054x - 1.551$	3.525 ± 0.018	0–14	0.981
1.5:1	$y = -0.091x - 1.606$	5.483 ± 0.017	0–14	0.991

3.2. *Effects of Arg on K-struvite formation kinetics*

Arg is a naturally occurring amino acid ubiquitously found in wastewater due to direct discharge from various sources and/or biological degradation of organic matter-containing proteins (i.e., protein metabolism) [49]. Understanding the effect of Arg on the K-struvite formation has practical implications for nutrient-recovering processes, as Arg (*pKa* values: 2.2, 9.0, and 12.5) retains its positive charge over most of the pH range encountered in batch experiments (i.e., 8.5 −10), ensuring continuous interaction with negatively-charged anions throughout the process. Similar batch experiments were performed in the presence of various levels of Arg and the results are shown in Fig. 2. Notably, the solution pH varied across different samples, with the blank sample (without Arg) exhibiting a moderate decrease in pH, while samples with lower Arg concentrations (2 and 5 mg L^{-1}) maintaining higher and more stable pH levels and sample with the highest Arg concentration (20 mg L^{-1}) leading to the most significant pH drop (Fig. 2a). This phenomenon is indicative of an inhibitory effect of Arg on the nucleation of K-struvite [50]. This strong inhibitory effect is also verified in Fig. 2b. Specifically, the blank sample showed a rapid drop in soluble PO_4^{3-}-P, indicating the formation of K-struvite. In contrast, all solutions containing Arg maintained significantly high levels of soluble phosphate throughout the experiments (above 10 mg L^{-1}), indicating a great inhibition of crystallization regardless of the concentration of Arg. This is due to the strong "covalent-like" electrostatic interactions between Arg and phosphate in solution [51], specifically the electrostatic interaction between the protonated guanidinium group of Arg and the negatively charged phosphate [52], which reduces the phosphate availability for the formation of K-struvite.

Consequently, the strong interaction between Arg and phosphate appears to yield poor kinetic fitting results (Table 2 and Fig. 2d–f), implying that the formation of K-struvite is unlikely to occur in a solution with a supersaturation of 0.47 in the presence of Arg. Noth that the solution with 5 mg L^{-1} of Arg showed an R^2 as high as 0.957, which appears to be irrelevant to K-struvite formation, as there is still a significant amount of phosphorus remaining in the solution and the pH is out of the optimal range (8–9.5) for K-struvite (Fig. 2b) [31,53]. However, the inhibitory effect of Arg has been significantly neutralized in solution with a higher supersaturation (i.e., 2.57, with Mg/P = 1:1, initial phosphate concentration ($C_{0,\ PO4}$) = 100 mg L^{-1}, equivalent to 1.053 mM, pH = 10), where K-struvite crystallization followed a well-defined first-order kinetics with a high coefficient (R^2) above 0.99 (Fig. 3, and Table S2). This observation confirms that high

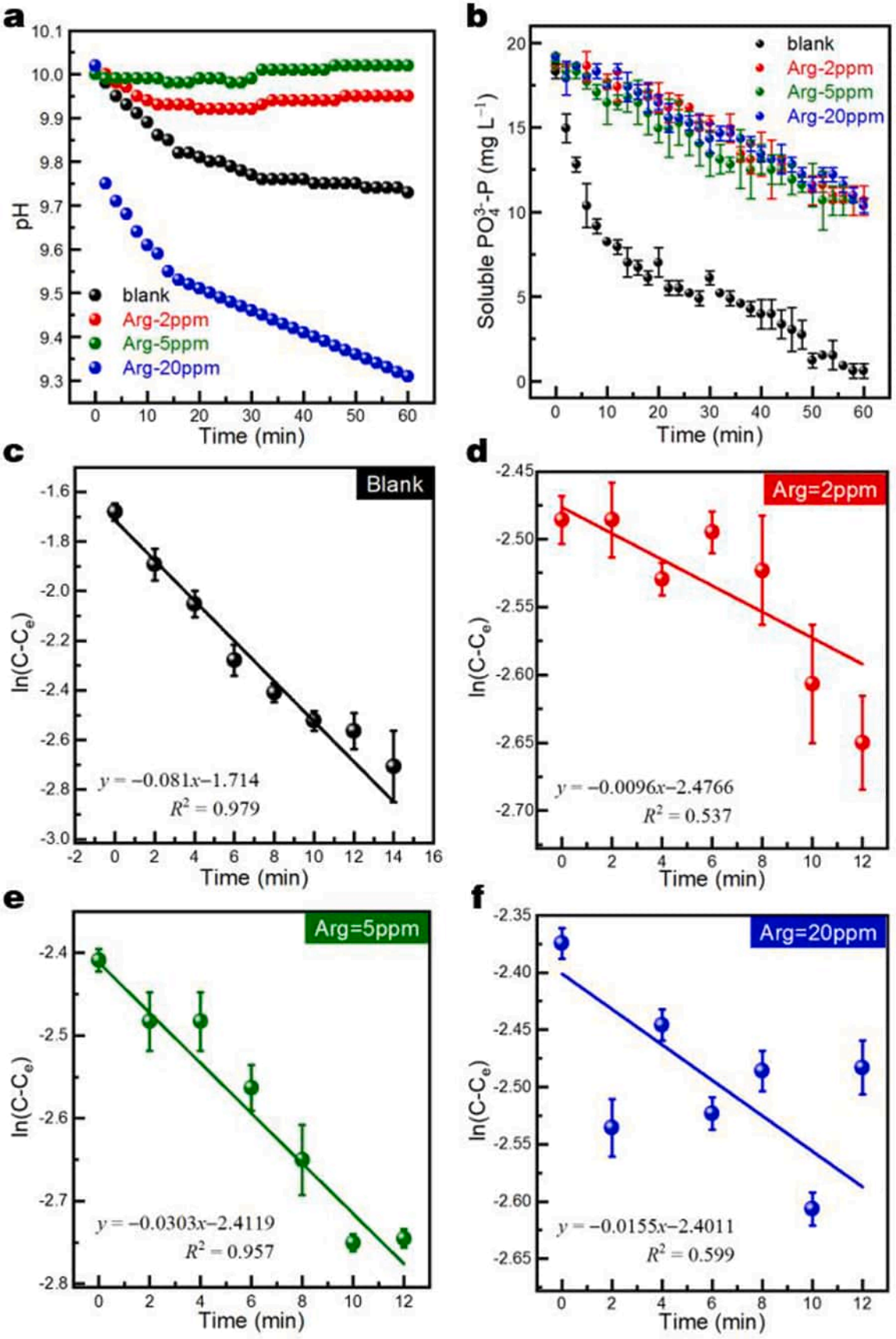

Fig. 2. (**a**) The solution pH profiles in solutions with 0.028 mM of PO_4^{3-}-P (Mg/P = 1:1) and varying contents of Arg, (**b**) Plots of soluble PO_4^{3-}-P versus reaction time, (**c-f**) Kinetic linear fitting plots of soluble phosphate concentration versus time in solutions containing (**c**) 0 (blank), (**d**) 2, (**e**) 5, and (**f**) 20 mg L^{-1} of L-arginine (Arg).

Table 2
Best-fit kinetic equations and corresponding parameters of K-struvite formation in BRs (Mg/P = 1:1) with varying contents of DOM impurities (Arg, CA, and HA) based on the first-order kinetic model.

Suspension code	Content (mg L^{-1})	First-order kinetic equation	k (h^{-1})	Time scale (min)	R^2
blank	0	$y = -0.081x - 1.714$	4.312 ± 0.317	0–14	0.979
Arg−2ppm	2	$y = -0.0096x - 2.4766$	0.583 ± 0.225	0–10	0.537
Arg−5ppm	5	$y = -0.0303x - 2.4119$	1.962 ± 0.231	0–10	0.957
Arg−20ppm	20	$y = -0.0155x - 2.4011$	1.251 ± 0.293	0–10	0.599
CA−5ppm	5	$y = -0.0226x - 2.5286$	1.373 ± 0.163	0–10	0.982
CA−20ppm	20	$y = -0.0114x - 2.4658$	0.688 ± 0.218	0–10	0.713
CA−50ppm	50	$y = -0.0139x - 2.4926$	0.728 ± 0.102	0–10	0.918
HA−5ppm	5	$y = -0.0150x - 2.5556$	0.599 ± 0.252	0–10	0.721
HA−20ppm	20	$y = -0.0235x - 2.5782$	1.560 ± 0.205	0–10	0.929
HA−50ppm	50	$y = -0.0273x - 3.0161$	1.793 ± 0.390	0–10	0.837

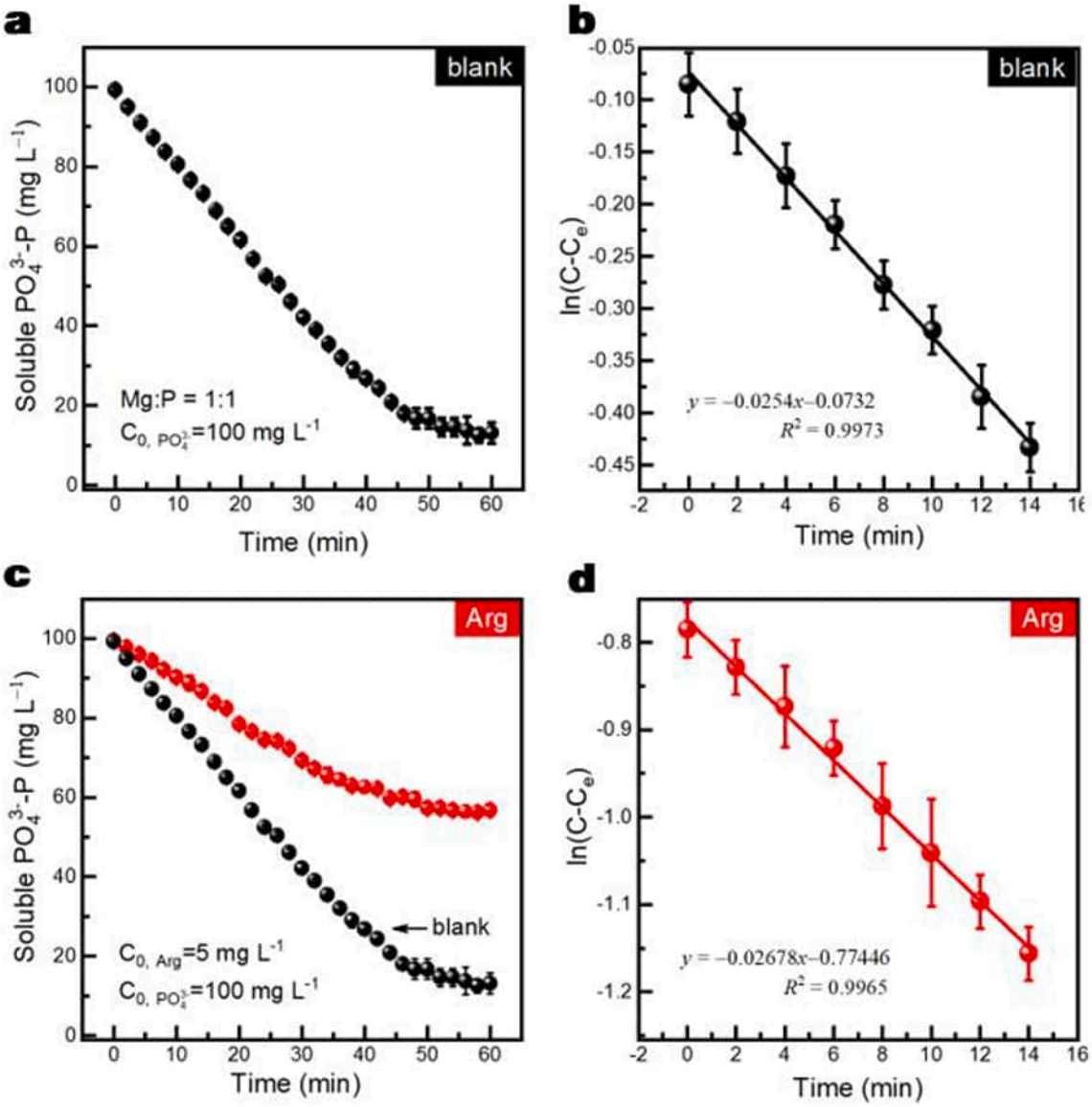

Fig. 3. (**a**, **c**) Plots of soluble PO_4^{3-}-P versus reaction time in (**a**) blank (Mg/P = 1:1, $C_{0,\ PO4}$ = 100 mg L^{-1}, equivalent to 1.053 mM) and (**c**) solution with 5 mg L^{-1} of Arg; (**b**, **d**) the corresponding kinetic linear fitting plots of soluble phosphate concentration versus time in (**b**) blank, and (**d**) solution with 5 mg L^{-1} of Arg. Note that the presence of 5 mg L^{-1} of Arg appears to restrain the rate of K-struvite crystallization to some degree, but did not alter the trend and manner of K-struvite formation that follows a well-defined first-order kinetic model as evidenced by the high coefficients (i.e., R^2 above 0.99).

supersaturation can play a key role in overcoming the inhibitory effects that DOMs exert on the crystallization of K-struvite [54]. Collectively, the strong inhibitory efficacy of Arg in solution with a low supersaturation (e.g., 0.47) is attributed to its high ability to suppress phosphate availability for K-struvite formation, which may pose challenges in recovering phosphate from wastewater containing such amino acids but highlights Arg's potential as an antifouling agent in industrial systems to prevent scaling.

3.3. Effects of CA on K-struvite formation kinetics

As a typical DOM originating from food industries, e.g., the orange juice production factories, CA is also ubiquitous in wastewater and contributes a high organic load (high chemical and biochemical oxygen demand) to the waste streams [55]. CA is believed to have a profound impact on struvite crystallization due to its high chelating ability toward cations [56]. Fig. S4 illustrates the effect of citric acid (5, 20, and 50 mg L^{-1}) on the formation of K-struvite. CA appears to lower solution pH significantly, even at a low concentration of 5 mg L^{-1}, due to its strong ability to release hydrogen ions (H^+) when dissolved in water (Fig. S4a) [55]. Specifically, in the presence of 5 mg L^{-1} of CA, the solution pH stabilized at approximately 7.5 after a 60-minute batch reaction, suggesting moderate inhibition. In contrast, the final pH was maintained around pH 8.0 in the case of the solution with 20 mg L^{-1} of CA, while the presence of 50 mg L^{-1} of CA caused a sharp drop below the required threshold (pH 8.5) to around 5, indicating strong inhibition of K-struvite formation at higher levels of CA.

Notably, most of the PO_4^{3-}-P is retained in solution in the presence of CA regardless of its concentration (Fig. S4b), confirming the inhibitory effect of CA on K-struvite formation within the time duration of the study (i.e., 60 min). The first-order kinetic fitting results showed that the correlation coefficients were 0.982, 0.713, and 0.918 for solutions containing 5, 20, and 50 mg L^{-1} of CA, respectively (Table 2 and Fig. S4c-e). However, given that the optimal pH range for K-struvite crystallization is between 8.0 and 9.5 [31], the reaction of K-struvite formation is only possible within 10 min in solutions with CA of 5 and 20 mg L^{-1}, respectively (Fig. S4a, c, d). In the presence of 5 mg L^{-1} CA, for instance, K-struvite formation is likely to occur within 10 min following a well-defined first-order kinetics as evidenced by the higher R^2 (i.e., 0.982). But afterward, CA adsorbs on the fresh crystal nuclei and appears to extract magnesium ions (Mg^{2+}), leading to the eventual dissolution of K-struvite nuclei [28,56]. Likewise, increasing supersaturation from 0.47 to 2.57 can effectively counteract the inhibitory effects of CA to a significant extent (Fig. S5), as evidenced by the well-defined first-order crystallization kinetics with higher coefficients (Table S2).

The major mechanism by which CA inhibits K-struvite crystallization involves the formation of citrate-magnesium complexes due to the high chelating ability of CA, which reduces the availability of free Mg^{2+} and K^+ ions required for K-struvite formation [31,56,57]. Additionally, CA appears to lower solution pH, shifting the equilibrium toward K-struvite dissolution rather than formation (Fig. S4a). This dissolution is exacerbated by CA's ability to protonate phosphate ions, reducing their availability for K-struvite crystallization [31]. Combinedly, CA primarily inhibits K-struvite formation in solution with a low supersaturation (e.g., 0.47) by lowering the solution pH unfavorable, and chelating Mg^{2+} and K^+ ions.

3.4. Effects of HA on K-struvite formation kinetics

Similarly, HA was also demonstrated to suppress the formation of struvite via a complex of interactions [20,58,59]. To evaluate the impact of HA molecules on K-struvite precipitation, we introduced HA at three levels (5, 20, and 50 mg L^{-1}) and investigated their effects on solution pH as well as the remaining phosphate (Fig. S6). Unlike our earlier observation in similar solutions for struvite crystallization showcasing a pH buffering effect of HA molecules [59], in the case of K-struvite formation, there was no pH buffering effect from HA, particularly at lower concentration (e.g., 5 mg L^{-1}, Fig. S6a). Namely, the presence of HA molecules appears to accelerate the pH drop, especially at lower HA levels. Interestingly, the introduction of 50 mg L^{-1} of HA molecules demonstrated a pH buffering effect but only after a 30-minute reaction. This is likely attributed to the difference in supersaturation stemming from the concentration of each component (e.g., 160 vs 20 mg L^{-1} in the case of phosphate) [28,59].

Likewise, in the presence of HA molecules, even the concentration of soluble phosphate decreased slightly with time as expected, but most of the soluble phosphate was retained in the solution (Fig. S6b), indicative of a strong inhibitory effect of HA on K-struvite crystallization. Note that all solution pH values fell out of the optimal crystallization pH range (> 9.5, Fig. S6a), indicating that K-struvite crystallization was unlikely to occur in solution with a supersaturation of 0.47 in the presence of HA. This is different from our earlier observation in solution with 160 mg L^{-1} of phosphate [59], implying a higher phosphate concentration and therefore higher supersaturation is necessary to drive K-struvite precipitation, particularly in the presence of HA. For this reason, the kinetic fitting failed to yield reasonable data (Table 2 and Fig. S6c-e), further confirming the strong inhibition of K-struvite crystallization by HA. However, a higher supersaturation level (e.g., 2.57) can effectively offset the inhibitory effects of HA on K-struvite formation (Fig. S5).

It is well known that HAs are complex organic macromolecules with various functional groups (e.g., carboxyl, carbonyl, phenolic hydroxyl, alcohol hydroxyl, amide, and amine, etc.), which play a crucial role in their reactivity, such as metal binding, solubility, and interactions with minerals or other organics [25–27,60,61]. To verify the surface adsorption between HA and K-struvite, zeta (ζ) potential measurements were conducted in diluted K-struvite suspensions in the absence or presence of HA over the pH range of 8–12. Notably, the presence of 5 mg L^{-1} of HA shifted the surface charge of K-struvite crystals to more negative values over the pH range (the cyan shaded region) favorable to K-struvite crystallization (Fig. 4), indicative of strong adsorption of HA onto the crystal surfaces since HA is much richer in negatively charged functional groups [59,60]. The increased surface negative charge, which, through enhanced electrostatic repulsion with negatively charged phosphate species as well as the negatively charged K-struvite nuclei, plays an inhibitory role in hindering the nucleation and continuous growth of K-struvite (i.e., inhibition by surface adsorption of DOMs) [62]. Similar trends were also observed for Arg and CA (Fig. 4), confirming the adsorption-based inhibition mechanism. In this context, the inhibitory role of HA in K-struvite formation in solution with a low supersaturation (e.g., 0.47) appears to involve multiple mechanisms: i) complexation and/or chelation of Mg^{2+} and K^+ ions [56,63], ii) surface adsorption and passivation of crystals [61], iii) lowering solution supersaturation [60,64], and iv) electrostatic stabilization of free phosphate [25,59,61].

3.5. Effects of DOMs on the precipitates reclaimed from BRs and FBRs

Apart from the crystallization kinetics, the effects of these DOMs on the properties of the reclaimed precipitates were also investigated subsequently. As mentioned above, K-struvite appears to form in BRs by following a well-defined first-order kinetics in the absence of any DOM impurities and at a Mg/P ratio of 1:1 (Fig. 1c). The precipitate from the above system was collected centrifugally, washed, and dried, and referred to as the blank sample. Note that the XRD pattern of the blank sample is featured by two diffuse humps over the 2θ range of 15 – 40° with an intensity trend well matched with the standard K-struvite (PDF # 35–0812) (Fig. 5a), indicating that the blank sample is poorly crystallized and likely predominated by amorphous phases and/or metastable nanocrystals [59,65]. This is likely attributed to the small

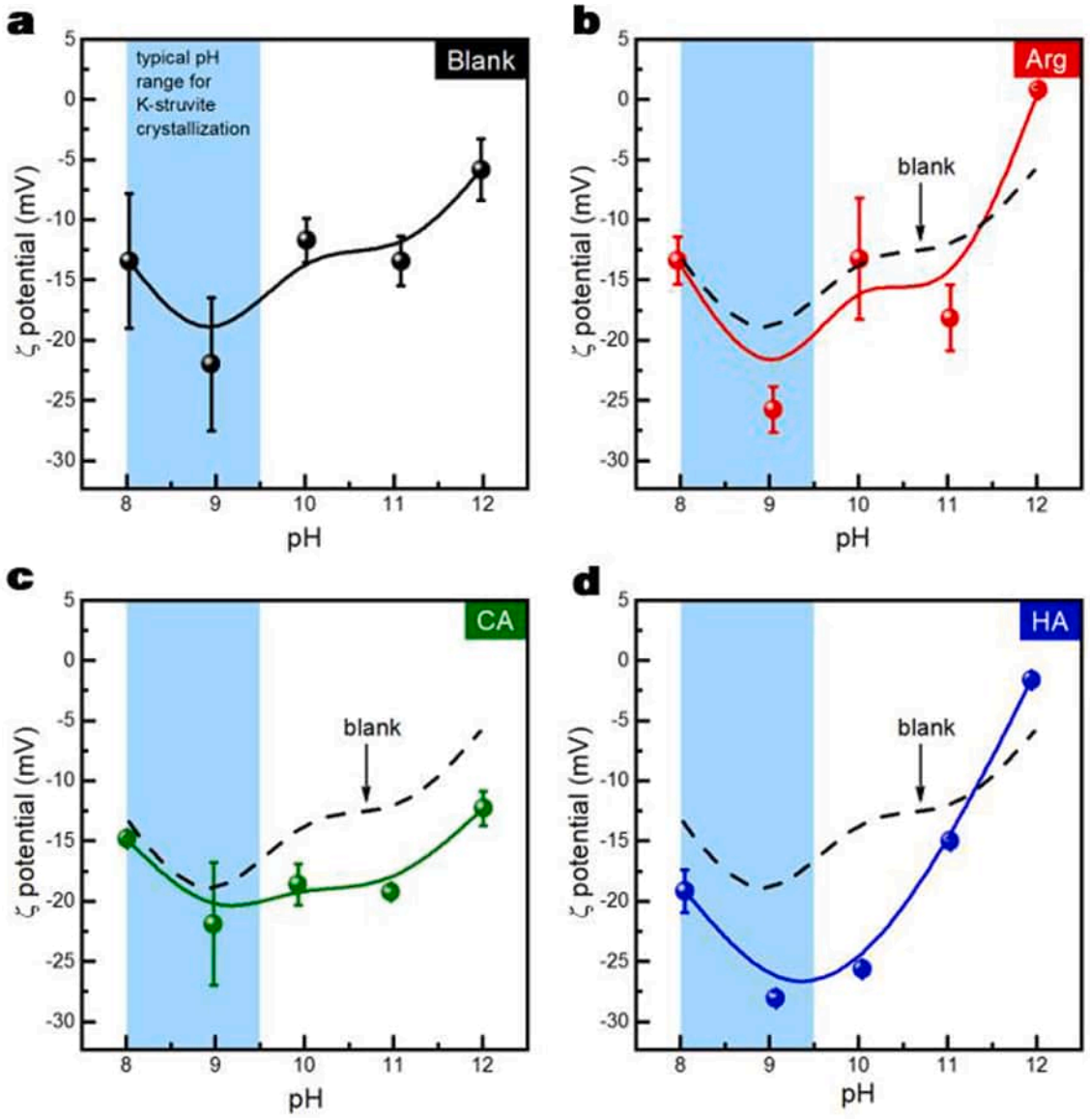

Fig. 4. Zeta (ζ) potential profiles of K-struvite: (**a**) blank (5 mg of K-struvite dispersed in 100 mL DI H_2O, w/o any DOMs), (**b**) with 5 mg L^{-1} of Arg, (**c**) with 5 mg L^{-1} of CA, and (**d**) with 5 mg L^{-1} of HA. ζ potential measurements were conducted in triplicate on a Zetasizer Nano ZS90 (Malvern, UK) under ambient conditions (25 °C, 1 atm). Note that the presence of Arg, CA, and HA shifted the surface charge of K-struvite crystals to more negative values over the pH range favorable to K-struvite crystallization, implying the adsorption of these DOMs on K-struvite and verifying the adsorption-based inhibition mechanism.

supersaturation (i.e., SI = 0.47) and the short crystallization time (i.e., 60 min) [30,31]. Other possible Mg-P phases, such as newberyite and bobierrite, are absent from the reclaimed precipitates, mainly since newberyite is formed only at pH < 6.5 [66], whereas bobierrite may form more slowly compared to K-struvite, despite being at a similar pH to that of K-struvite [67]. Infrared spectroscopic analysis (Fig. 5b) also confirmed the formation of K-struvite with typical IR bands assignable to hydroxyl groups ($\nu_{\text{-OH}}$ at 3423 cm^{-1}, and δ_{H2O} at 1634 cm^{-1}), phosphate (ν_3 at 1062 cm^{-1}, and ν_4 at 575 cm^{-1}), and metal-oxygen band (Mg-O), respectively [31,68–70]. SEM images reveal that the poorly crystallized K-struvite was irregularly shaped particulates with a broad size variation from several to tens of μm (Fig. 5c, d). Unlike the well-defined wedge-shaped or cuboid morphology observed in K-struvite prepared hydrothermally [30], the blank sample appears to be dominated by amorphous aggregates (see the yellow dashed box) with minor flat tabular crystals (highlighted with yellow arrows, Fig. 5c, d) [71], in good consistency with the above XRD data. Unfortunately, any attempts to centrifugally separate the precipitates from solutions in the presence of any DOMs (e.g., Arg, CA, and HA) failed due to their strong inhibitory effects on K-struvite crystallization (Figs. 2, S4 and S6) as well as the unfavorable solution conditions observed in the blank system (i.e., low SI, and short duration). Nevertheless, when a higher supersaturation (i.e., 2.57 with a Mg/P ratio of 1:1 and $C_{0,\ PO4}$ of 100 mg L^{-1}) was applied, poorly crystallized K-struvite was formed regardless of the presence of these DOMs of 5 mg L^{-1} (Fig. S7), confirming the above observation in kinetic studies that a higher supersaturation can effectively counteract the inhibition from DOMs (Figs. 3 and S5).

To evaluate the effects of naturally occurring DOMs (represented by the chemical oxygen demand (COD) values for simplicity) on the reclaimed precipitates in an FBR, we also harvested and characterized the settleable solids from the bottom of the custom-built FBR fed mainly with a real sludge dewatering liquid (Table S1). Crystallographic analysis indicates that the reclaimed precipitate appears to consist of poorly crystallized K-struvite (PDF #35–0812), vivianite (PDF #30–0662) and a majority of amorphous phase (Fig. S8a) probably due to the combined actions from the inhibition of natural DOMs (i.e., 187 mg L^{-1} of COD)

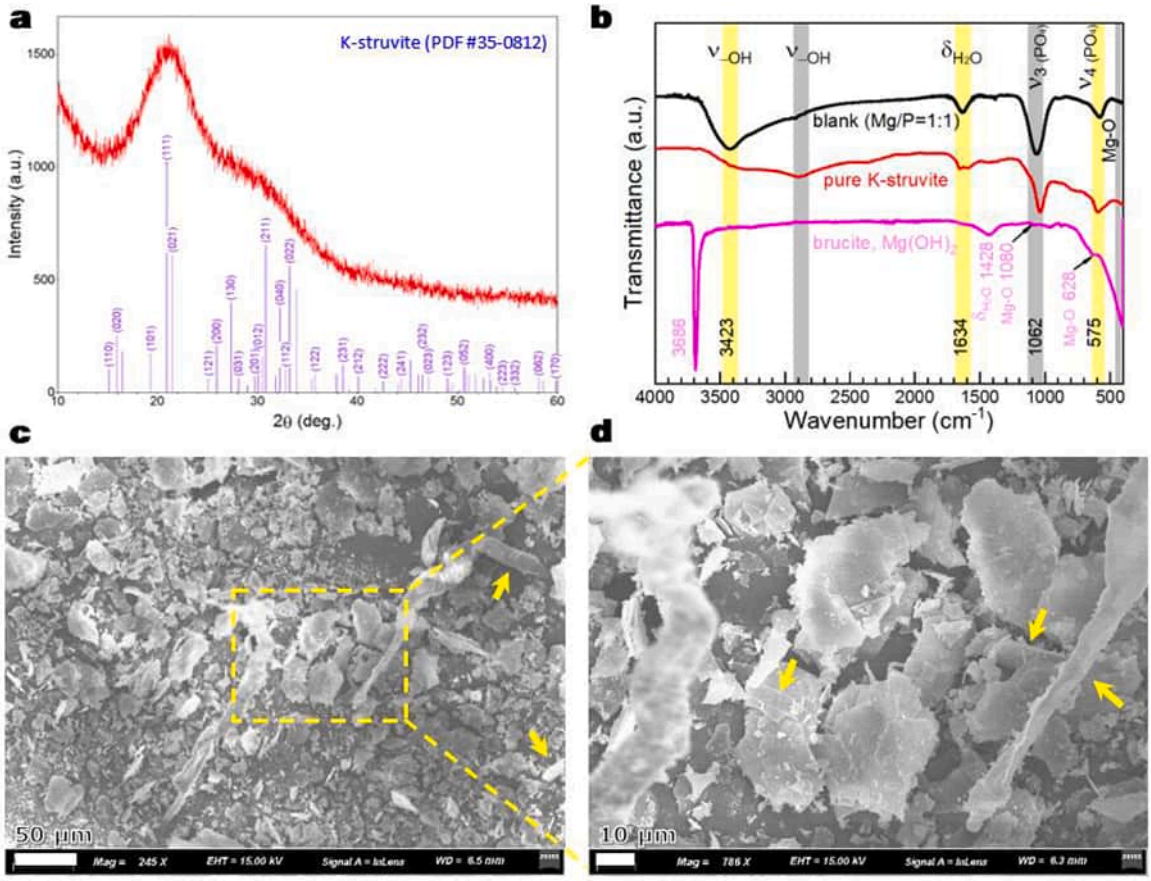

Fig. 5. Characterization of the reclaimed precipitate obtained from a BR with a Mg/P molar ratio of 1:1: (**a**) XRD pattern, (**b**) FTIR spectrum verifying the presence of K-struvite and the absence of brucite (*cf*. the standard brucite infrared data—the light magenta curve in panel **b**—is obtained from the RRUFF™ project database, https://www.rruff.net/, while the infrared data of pure K-struvite is from [70]), and (**c**, **d**) SEM images (note: yellow arrows highlight the rodlike K-struvite).

and the competition from the complex co-occurring ions (Table S1), which is also substantiated by the corresponding FTIR analysis (Fig. S8b). Further studies are required to specify the underlying mechanism regulating phase compositions in FBRs with real wastewater as feed solutions. Interestingly, the precipitate appears to be dominated by irregularly shaped aggregates, hexagon-shaped crystals (see the blue hexagons, Fig. S8c), and radiative shuttle-shaped crystals (highlighted with yellow arrows, Fig. S8d), which are assignable to the amorphous phase, K-struvite and vivianite crystals, respectively, according to earlier reports [30,72]. Given the high SI of 2.53 in the FBR feed solution (Text S1, Supporting Information) and the crystallization period of up to 6 days, these favorable conditions for crystallization will undoubtedly counteract in part the inhibition induced by coexisting DOMs, thus yielding crystals with a more regular morphology (Fig. S8c, d). Collectively, a low SI and short reaction time in BR systems are unfavorable for the formation of high crystallinity K-struvite, although the precipitation reaction is facilitated. The presence of any DOMs can completely hinder the precipitation reaction. In contrast, in FBR matrices, the high SI and long reaction time can partially counteract the inhibitory effect of DOMs, thus promoting the formation of crystals with regular morphology. However, the presence of foreign ions (e.g., Ca^{2+}, Fe^{3+}, etc.) in actual wastewater resulted in a decrease in the purity of the reclaimed K-struvite [38,73]. Further studies are needed to alleviate the interference of such foreign ions.

3.6. Roles of DOMs on K-struvite formation in BRs and FBRs

Recall that different DOMs have varying functional groups, which usually act as binding sites or domains towards different species (i.e., chelation or complexation with ions), thereby significantly influencing K-struvite crystallization in both BRs and FBRs. To illustrate the DOM-specific specific domains, we performed a structural optimization for the electrostatic potential maps of all three DOMs by using GaussView 6.0 [74] software (Fig. 6). For instance, Arg is featured by guanidinium, amine, and carboxylic groups (see the blue, orange and red ovals, respectively in Fig. 6a). The positively charged guanidinium group ($-NH-C(NH_2)_2^+$, see the lower-left blue domain in Fig. 6b) is believed to bind anions e.g., PO_4^{3-} and HPO_4^{2-} (i.e., complexation of anions) [75]. Contrastingly, a CA molecule has three negatively charged carboxyl groups (–COO^-, red domains in Fig. 6d) that are likely to form strong complexes with Mg^{2+} and K^+ (i.e., charge-mediated complexation of cations) [57]. In the case of HA, it is rich in both the positively charged and the negatively charged groups (see the molecular structure of HA based on the Stevenson model (Fig. 6e) [76], and the blue and red domains in Fig. 6f), which can attract both the cations and the anions [31,32]. Besides, the heterogeneous surface with phenolic/carboxyl motifs of HA can chelate Mg^{2+} or K^+ ions via polydentate binding (i.e., chelation of cations) [56,63]. These interactions dominate over ion-pair formation, thereby limiting ions' mobility and hindering K-struvite precipitation.

Moreover, acidic DOMs (e.g., CA and HA) release H^+ when interacting with water, lowering solution pH to ≤ 7.0 in most situations. However, K-struvite crystallization favors alkaline conditions (i.e., pH 8–10), where PO_4^{3-} dominates. Nevertheless, pH depression in the presence of acidic DOMs is likely to shift phosphate speciation toward $HPO_4^{2-}/H_2PO_4^-$, reducing phosphate availability and therefore impeding nucleation and crystal growth of K-struvite [55]. Additionally, DOMs are likely to adsorb onto the active growth sites or the nuclei of K-struvite

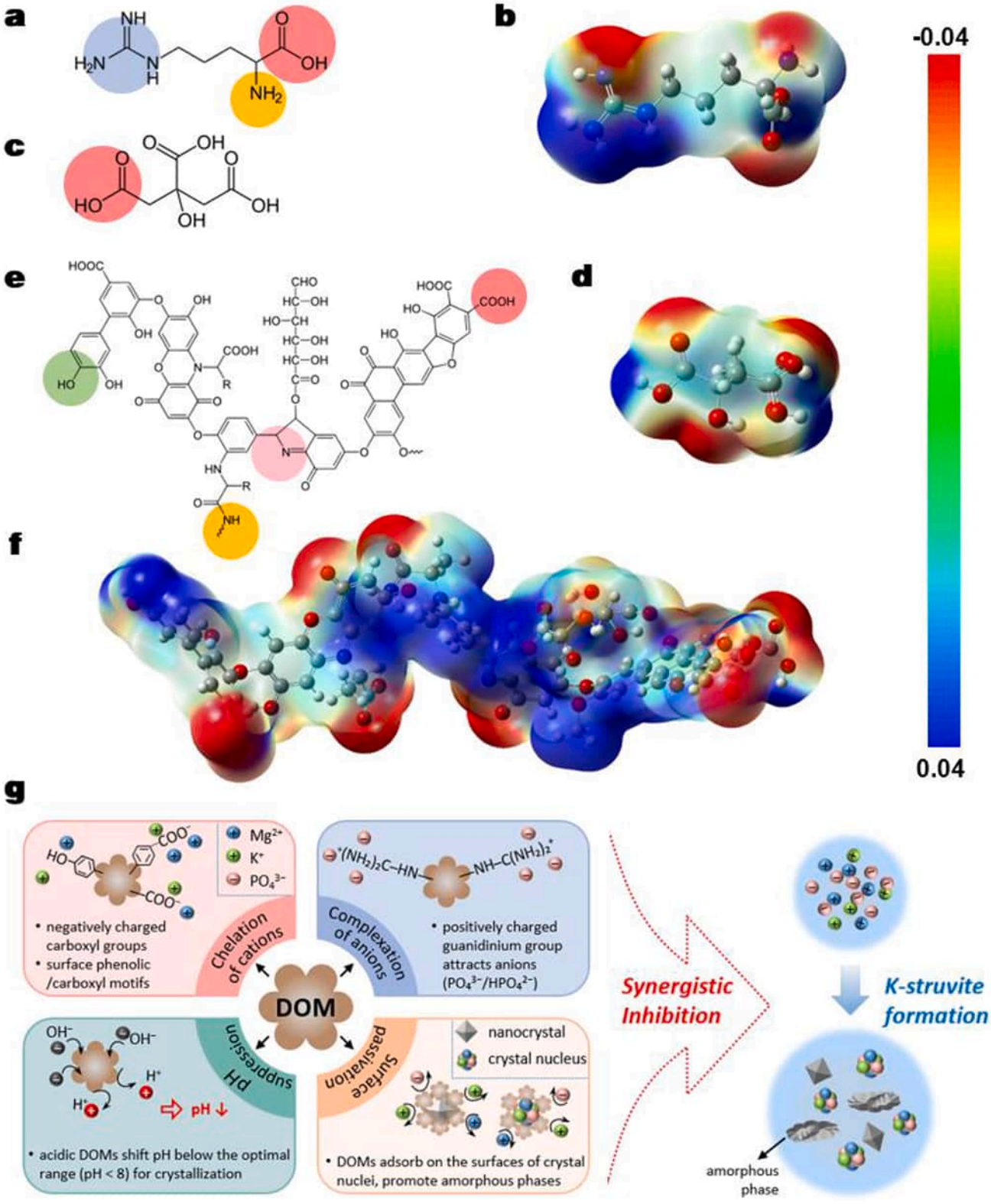

Fig. 6. The molecular structures and the corresponding electrostatic potentials of all these DOMs studied. (**a**, **b**) Arg, (**c**, **d**) CA, and (**e**, **f**) HA based on the Stevenson model. The ovals represent key moieties within DOMs: red for carboxylic groups, blue for guanidinium groups, green for phenolic groups, orange for amine or amide groups, and pink for nitrogen heterocycles. (**g**) The proposed roles of DOMs in suppressing the formation of K-struvite.

crystals, blocking further ion attachment (i.e., surface adsorption and passivation) [25]. This appears to disrupt crystal lattice formation, leading to smaller, defective, or amorphous precipitates rather than well-defined crystals, which has also been observed in our current work (Figs. 5 and S8). Collectively, DOMs universally disrupt K-struvite formation via distinct mechanisms: i) chelation of cations, ii) complexation of anions, iii) pH suppression, and iv) surface adsorption and passivation of crystal nuclei (Fig. 6g). Specifically, negatively charged DOMs (e.g., CA and HA molecules) sequester Mg^{2+} or K^{+} ions and depress pH, while cationic Arg immobilizes phosphate. Besides, all these DOMs can adsorb and passivate the surface of crystal nuclei or active sites for crystal growth, hindering K-struvite growth and promoting the formation of amorphous precipitates. All these key mechanisms are likely to occur simultaneously, thus leading to synergistic inhibition of K-struvite formation. In this regard, optimizing K-struvite recovery requires DOM-specific pretreatment (e.g., pH adjustment, selective oxidation) to mitigate complexation and stabilize ideal crystallization conditions, which needs to be further explored in follow-up investigations.

4. Conclusion

In this study, three organic acids, i.e., Arg, CA, and HA, were employed as typical DOM-type impurities in phosphate-containing solution for systematically assessing their effects on K-struvite formation in both the batch and the fluidized-bed reactors. Our batch crystallization results indicate that, in the absence of any DOMs, K-struvite formation followed a well-defined first-order kinetic with correlation coefficients above 0.98, and that a higher Mg/P molar ratio appears to drive a much faster kinetics over the range of 1:1 – 1.5:1. In the presence of Arg, however, K-struvite precipitation was strongly hindered due to the high affinity of Arg towards phosphate ions, leading to poor kinetic modeling data. Likewise, the presence of citric or humic acids also significantly suppressed the formation of K-struvite by lowering the solution pH values unfavorable for K-struvite crystallization, and capturing Mg^{2+} and K^{+} by electrostatic attraction or chelation, resulting in poor kinetic modeling results too. Moreover, it has been shown experimentally that the DOM-free solution with a lower supersaturation in batch reactors seems to yield a precipitate dominated by amorphous phase along with poorly crystallized K-struvite, while the presence of naturally occurring DOMs also altered the phase compositions and morphology of the precipitates from the fluidized-bed reactors, yielding a mixture of amorphous precipitates and a few hexagonal K-struvite and shuttle-shaped vivianite. Additionally, electrostatic potential mapping analysis reveals that all these DOMs significantly influenced the formation of K-struvite via varying interactions between their surface functional groups and the species in solution, such as i) chelation of cations, ii) complexation of anions, iii) pH suppression, and iv) surface adsorption and passivation of tiny crystals or nuclei. However, further research would be required to underpin these mechanisms at the molecular level and to tackle and mitigate the inhibition of DOM-type impurities to improve phosphorus sustainability. These insights can initiate strategies that address the inhibitory effects of DOMs and stabilize an optimal condition for K-struvite recovery from real wastewater streams.

CRediT authorship contribution statement

Muhammad Bilal Zahid: Writing – original draft, Visualization, Methodology, Investigation. **Xianfei Wang:** Methodology, Investigation. **Yangfan Xia:** Visualization, Investigation. **Xinyi Xu:** Investigation. **Dawei Li:** Writing – review & editing, Resources. **Feihu Li:** Writing – review & editing, Writing – original draft, Supervision, Project administration, Conceptualization.

Declaration of Competing Interest

The authors declare that they have no known competing financial interests or personal relationships that could have appeared to influence the work reported in this paper.

Acknowledgements

We are grateful to the National Natural Science Foundation for financial support (NSFC 52000101, 42577076) and to Nanjing Qiaobei WWTP for providing the sludge dewatering liquid for our FBR experiments. M. B. Zahid is thankful to the China Scholarship Council (CSC) for financial support of his Postgraduate programme (2023GSP007233).

Appendix A. Supporting information

Supplementary data associated with this article can be found in the online version at doi:10.1016/j.jece.2025.118515.

Data availability

Data will be made available on request.

References

[1] C.T. Reinhard, N.J. Planavsky, B.C. Gill, K. Ozaki, L.J. Robbins, T.W. Lyons, W. W. Fischer, C.J. Wang, D.B. Cole, K.O. Konhauser, Evolution of the global phosphorus cycle, Nature 541 (2017) 386–389, https://doi.org/10.1038/nature20772.
[2] C. Alewell, B. Ringeval, C. Ballabio, D.A. Robinson, P. Panagos, P. Borrelli, Global phosphorus shortage will be aggravated by soil erosion, Nat. Commun. 11 (2020) 4546, https://doi.org/10.1038/s41467-020-18326-7.
[3] D. Cordell, J.O. Drangert, S. White, The story of phosphorus: global food security and food for thought, Glob. Environ. Chang. 19 (2009) 292–305, https://doi.org/10.1016/j.gloenvcha.2008.10.009.
[4] D.P. Van Vuuren, A.F. Bouwman, A.H.W. Beusen, Phosphorus demand for the 1970-2100 period: a scenario analysis of resource depletion, Glob. Environ. Chang. 20 (2010) 428–439, https://doi.org/10.1016/j.gloenvcha.2010.04.004.
[5] A.R. Jupp, S. Beijer, G.C. Narain, W. Schipper, J.C. Slootweg, Phosphorus recovery and recycling - closing the loop, Chem. Soc. Rev. 50 (2021) 87–101, https://doi.org/10.1039/d0cs01150a.
[6] S. Yeoman, T. Stephenson, J.N. Lester, R. Perry, The removal of phosphorus during wastewater treatment - a review, Environ. Pollut. 49 (1988) 183–233, https://doi.org/10.1016/0269-7491(88)90209-6.
[7] B.L. Wu, J. Wan, Y.Y. Zhang, B.C. Pan, I.M.C. Lo, Selective phosphate removal from water and wastewater using sorption: process fundamentals and removal mechanisms, Environ. Sci. Technol. 54 (2020) 50–66, https://doi.org/10.1021/acs.est.9b05569.
[8] D. Tonini, H.G.M. Saveyn, D. Huygens, Environmental and health co-benefits for advanced phosphorus recovery, Nat. Sustain. 2 (2019) 1051–1061, https://doi.org/10.1038/s41893-019-0416-x.
[9] L.E. de-Bashan, Y. Bashan, Recent advances in removing phosphorus from wastewater and its future use as fertilizer (1997-2003), Water Res. 38 (2004) 4222–4246, https://doi.org/10.1016/j.watres.2004.07.014.
[10] E. Desmidt, K. Ghyselbrecht, Y. Zhang, L. Pinoy, B. Van der Bruggen, W. Verstraete, K. Rabaey, B. Meesschaert, Global phosphorus scarcity and Full-Scale P-Recovery techniques: a review, Crit. Rev. Environ. Sci. Technol. 45 (2015) 336–384, https://doi.org/10.1080/10643389.2013.866531.
[11] B.K. Mayer, L.A. Baker, T.H. Boyer, P. Drechsel, M. Gifford, M.A. Hanjra, P. Parameswaran, J. Stoltzfus, P. Westerhoff, B.E. Rittmann, Total value of phosphorus recovery, Environ. Sci. Technol. 50 (2016) 6606–6620, https://doi.org/10.1021/acs.est.6b01239.
[12] K.S. Le Corre, E. Valsami-Jones, P. Hobbs, S.A. Parsons, Phosphorus recovery from wastewater by struvite crystallization: a review, Crit. Rev. Environ. Sci. Technol. 39 (2009) 433–477, https://doi.org/10.1080/10643380701640573.
[13] S. Kataki, H. West, M. Clarke, D.C. Baruah, Phosphorus recovery as struvite: recent concerns for use of seed, alternative mg source, nitrogen conservation and fertilizer potential, Resour. Conserv. Recycl. 107 (2016) 142–156, https://doi.org/10.1016/j.resconrec.2015.12.009.
[14] B. Li, I. Boiarkina, W. Yu, H.M. Huang, T. Munir, G.Q. Wang, B.R. Young, Phosphorous recovery through struvite crystallization: challenges for future design, Sci. Total Environ. 648 (2019) 1244–1256, https://doi.org/10.1016/j.scitotenv.2018.07.166.
[15] H.M. Huang, J. Li, B. Li, D.D. Zhang, N. Zhao, S.F. Tang, Comparison of different K-struvite crystallization processes for simultaneous potassium and phosphate recovery from source-separated urine, Sci. Total Environ. 651 (2019) 787–795, https://doi.org/10.1016/j.scitotenv.2018.09.232.

[16] A.F.R. Silva, Y.A.R. Lebron, Y.L. Brasil, L.C. Lange, M.C.S. Amaral, Effect of electrolyte solution recycling on the potassium recovery from vinasse by integrated electrodialysis and K-struvite precipitation processes, Chem. Eng. J. 450 (2022) 137975, https://doi.org/10.1016/j.cej.2022.137975.
[17] T. Zhou, N.G. Xu, G.Y. Chen, M. Zhang, T. Ji, X. Feng, C.S. Wang, Magnesium source with function of slowly releasing mg and ph control for impurity-resistance synthesis ultra-large struvite from wastewater, Sci. Total Environ. 924 (2024) 171636, https://doi.org/10.1016/j.scitotenv.2024.171636.
[18] A. Rabinovich, A.A. Rouff, Effect of phenolic organics on the precipitation of struvite from simulated dairy wastewater, ACS EST Water 1 (2021) 910–918, https://doi.org/10.1021/acsestwater.0c00234.
[19] A. Rabinovich, A.A. Rouff, Changes to struvite growth and morphology as impacted by low molecular weight organics, ACS EST Water 3 (2023) 2277–2285, https://doi.org/10.1021/acsestwater.3c00062.
[20] J.N. Yan, M.Y. Ma, F.H. Li, Revealing the Roles of Microplastics and Dissolved Organic Matter in Phosphorus Recovery via Struvite Crystallization in Batch and Fluidized-Bed Reactors, ChemRxiv (2024), https://doi.org/10.26434/chemrxiv-2024-cr2vg.
[21] A. Capdevielle, E. Sykorova, F. Beline, M.L. Daumer, Effects of organic matter on crystallization of struvite in biologically treated swine wastewater, Environ. Technol. 37 (2016) 880–892, https://doi.org/10.1080/09593330.2015.1088580.
[22] A. Muhmood, X.Q. Wang, R.J. Dong, S.B. Wu, New insights into interactions of organic substances in poultry slurry with struvite formation: an overestimated concern? Sci. Total Environ. 751 (2021) 141789 https://doi.org/10.1016/j.scitotenv.2020.141789.
[23] M.H. Yao, L.Y. Wang, J.H. Wei, Z.K. Cen, X.M. Wei, G.Q. Yu, H.L. Shen, R.P. Shen, D.D. Han, M.Y. Chen, K.L. Li, J.B. Gong, Effects of organic pollutants on struvite crystallization kinetics and the molecular mechanism of inhibition on crystal growth, Sci. Total Environ. 894 (2023) 164882, https://doi.org/10.1016/j.scitotenv.2023.164882.
[24] Y.Y. Lou, Z.L. Ye, S.H. Chen, Q.S. Wei, J.Q. Zhang, X. Ye, Influences of dissolved organic matters on tetracyclines transport in the process of struvite recovery from swine wastewater, Water Res. 134 (2018) 311–326, https://doi.org/10.1016/j.watres.2018.02.010.
[25] Z.L. Ye, J.Q. Zhang, J.S. Cai, S.H. Chen, Investigation of tetracyclines transport in the presence of dissolved organic matters during struvite recovery from swine wastewater, Chem. Eng. J. 385 (2020) 123950, https://doi.org/10.1016/j.cej.2019.123950.
[26] L. Wei, T.Q. Hong, K.P. Cui, T.H. Chen, Y.F. Zhou, Y.X. Zhao, Y.D. Yin, J.F. Wang, Q. Zhang, Probing the effect of humic acid on the nucleation and growth kinetics of struvite by constant composition technique, Chem. Eng. J. 378 (2019) 122130, https://doi.org/10.1016/j.cej.2019.122130.
[27] Z. Zhou, L. Hu, W.C. Ren, Y.Z. Zhao, L.M. Jiang, L.C. Wang, Effect of humic substances on phosphorus removal by struvite precipitation, Chemosphere 141 (2015) 94–99, https://doi.org/10.1016/j.chemosphere.2015.06.089.
[28] A.N. Kofina, K.D. Demadis, P.G. Koutsoukos, The effect of citrate and phosphocitrate on struvite spontaneous precipitation, Cryst. Growth Des. 7 (2007) 2705–2712, https://doi.org/10.1021/cg0603927.
[29] J. Prywer, E. Mielniczek-Brzoska, M. Olszynski, Struvite crystal growth inhibition by trisodium citrate and the formation of chemical complexes in growth solution, J. Cryst. Growth 418 (2015) 92–101, https://doi.org/10.1016/j.jcrysgro.2015.02.027.
[30] L.J. Gardner, S.A. Walling, S.M. Lawson, S.K. Sun, S.A. Bernal, C.L. Corkhill, J. L. Provis, D.C. Apperley, D. Iuga, J.V. Hanna, N.C. Hyatt, Characterization of and structural insight into Struvite-K, $KMgPO_4{\cdot}6H_2O$, an analogue of struvite, Inorg. Chem. 60 (2021) 195–205, https://doi.org/10.1021/acs.inorgchem.0c02802.
[31] I. Kabdasli, A. Siciliano, C. Limonti, O. Tünay, Is K-Struvite precipitation a plausible nutrient recovery method from Potassium-Containing Wastes?-A review, Sustainability 14 (2022) 11680, https://doi.org/10.3390/su141811680.
[32] L. Wei, Y.M. Tang, T.T. Zhang, J.J. Ji, Q. Zhang, Y.G. Dong, L. Luo, X.K. Ding, J. Y. Kong, Factors influencing K-struvite purity via phosphorus coprecipitation in synthetic urine: verification, quantification, and modelling, Environ. Res. 264 (2025) 120346, https://doi.org/10.1016/j.envres.2024.120346.
[33] J.A. Leenheer, J.P. Croué, Characterizing aquatic dissolved organic matter, 18a-26a, Environ. Sci. Technol. 37 (2003), https://doi.org/10.1021/es032333c.
[34] Y.F. Shi, S.N. Li, L.Y. Wang, J.C. Li, G.C. Shen, G. Wu, K. Xu, H.Q. Ren, J.J. Geng, Characteristics of DOM in 14 AAO processes of municipal wastewater treatment plants, Sci. Total Environ. 742 (2020) 140654, https://doi.org/10.1016/j.scitotenv.2020.140654.
[35] H. Lin, K. Matsui, R.J. Newton, L.D. Guo, Disproportionate changes in composition and molecular size spectra of dissolved organic matter between influent and effluent from a major metropolitan wastewater treatment plant, ACS EST Water 2 (2022) 216–225, https://doi.org/10.1021/acsestwater.1c00391.
[36] A.C. Maizel, C.K. Remucal, The effect of advanced secondary municipal wastewater treatment on the molecular composition of dissolved organic matter, Water Res. 122 (2017) 42–52, https://doi.org/10.1016/j.watres.2017.05.055.
[37] S.O. Abayie, L. Rautio, T. Kauppinen, T. Hu, S. Tuomikoski, J. Pesonen, K-Struvite precipitation from source-separated battery wastewater, J. Environ. Chem. Eng. 13 (2025) 117323, https://doi.org/10.1016/j.jece.2025.117323.
[38] I. Kabdasli, S. Kuscuoglu, O. Tunay, A. Siciliano, Assessment of K-Struvite precipitation as a means of nutrient recovery from source separated human urine, Sustainability 14 (2022) 1082, https://doi.org/10.3390/su14031082.
[39] F.H. Li, W.H. Wu, R.Y. Li, X.R. Fu, Adsorption of phosphate by acid-modified Fly ash and palygorskite in aqueous solution: experimental and modeling, Appl. Clay Sci. 132 (2016) 343–352, https://doi.org/10.1016/j.clay.2016.06.028.
[40] D. Wang, W.L. Ye, G.X. Wu, R.Q. Li, Y.R. Guan, W. Zhang, J.X. Wang, Y.L. Shan, K. Hubacek, Greenhouse gas emissions from municipal wastewater treatment facilities in China from 2006 to 2019, Sci. Data 9 (2022) 317, https://doi.org/10.1038/s41597-022-01439-7.
[41] N.O. Nelson, R.L. Mikkelsen, D.L. Hesterberg, Struvite precipitation in anaerobic swine lagoon liquid: effect of ph and mg: p ratio and determination of rate constant, Bioresour. Technol. 89 (2003) 229–236, https://doi.org/10.1016/S0960-8524(03)00076-2.
[42] V.G. Le, C.T. Vu, Y.J. Shih, X.T. Bui, C.H. Liao, Y.H. Huang, Phosphorus and potassium recovery from human urine using a fluidized bed homogeneous crystallization (FBHC) process, Chem. Eng. J. 384 (2020) 123282, https://doi.org/10.1016/j.cej.2019.123282.
[43] X.N. Liu, G.Q. Wen, Z.Y. Hu, J. Wang, Coupling effects of ph and Mg/P ratio on p recovery from anaerobic digester supernatant by struvite formation, J. Clean. Prod. 198 (2018) 633–641, https://doi.org/10.1016/j.jclepro.2018.07.073.
[44] J.Z. Wu, Y.F. Li, B.J. Xu, M. Li, J. Wang, Y.N. Shao, F.Y. Chen, M. Sun, B. Liu, Effects of physicochemical parameters on struvite crystallization based on kinetics, Int. J. Environ. Res. Public Health 19 (2022) 7204, https://doi.org/10.3390/ijerph19127204.
[45] J. Hovelmann, C.V. Putnis, In situ nanoscale imaging of struvite formation during the dissolution of natural brucite: implications for phosphorus recovery from wastewaters, Environ. Sci. Technol. 50 (2016) 13032–13041, https://doi.org/10.1021/acs.est.6b04623.
[46] H.M. Huang, D.D. Zhang, W.J. Wang, B. Li, N. Zhao, J. Li, J.K. Dai, Alleviating Na^+ effect on phosphate and potassium recovery from synthetic urine by K-struvite crystallization using different magnesium sources, Sci. Total Environ. 655 (2019) 211–219, https://doi.org/10.1016/j.scitotenv.2018.11.259.
[47] N. Marti, A. Bouzas, A. Seco, J. Ferrer, Struvite precipitation assessment in anaerobic digestion processes, Chem. Eng. J. 141 (2008) 67–74, https://doi.org/10.1016/j.cej.2007.10.023.
[48] K.N. Xu, C.W. Wang, H.Y. Liu, Y. Qian, Simultaneous removal of phosphorus and potassium from synthetic urine through the precipitation of magnesium potassium phosphate hexahydrate, Chemosphere 84 (2011) 207–212, https://doi.org/10.1016/j.chemosphere.2011.04.057.
[49] M.H. Liu, J.H. Huang, Y. Deng, Adsorption behaviors of L-arginine from aqueous solutions on a spherical cellulose adsorbent containing the sulfonic group, Bioresour. Technol. 98 (2007) 1144–1148, https://doi.org/10.1016/j.biortech.2006.03.026.
[50] J.S. Hu, C. Hong, Z.X. Li, Y. Xing, Z.X. Zheng, X.M. Zhao, Z.Q. Wang, H.J. Zhao, Z. Zhang, J. Meng, C.H. Qi, Nitrogen release of hydrothermal treatment of antibiotic fermentation residue and preparation of struvite from hydrolysate, Sci. Total Environ. 713 (2020) 135174, https://doi.org/10.1016/j.scitotenv.2019.135174.
[51] A.S. Woods, S. Ferré, Amazing stability of the arginine-phosphate electrostatic interaction, J. Proteome Res. 4 (2005) 1397–1402, https://doi.org/10.1021/pr050077s.
[52] A.S.H. Hameed, G. Ravi, M.D.M. Hossain, P. Ramasamy, Growth and characterisation of L-arginine phosphate family crystals, J. Cryst. Growth 204 (1999) 333–340, https://doi.org/10.1016/S0022-0248(99)00173-6.
[53] V.B. Aguilar-Pozo, J.M. Chimenos, B. Elduayen-Echave, K. Olaciregui-Arizmendi, A. López, J. Gómez, M. Guembe, I. García, E. Ayesa, S. Astals, Struvite precipitation in wastewater treatment plants anaerobic digestion supernatants using a magnesium oxide by-product, Sci. Total Environ. 890 (2023) 164084, https://doi.org/10.1016/j.scitotenv.2023.164084.
[54] S. Shaddel, S. Ucar, J.P. Andreassen, S.W. Osterhus, Engineering of struvite crystals by regulating supersaturation - correlation with phosphorus recovery, crystal morphology and process efficiency, J. Environ. Chem. Eng. 7 (2019) 102918, https://doi.org/10.1016/j.jece.2019.102918.
[55] W.H. Liu, Z.Y. Zheng, F.X. Sun, M.D. Miao, M.H. Cui, H.B. Liu, H.M. Zhang, C. Zhang, Z.J. Hu, H. Liu, Valorization of citric acid production wastewater as alternative carbon source for biological nutrients removal: a pilot-scale case study, J. Clean. Prod. 258 (2020) 120576, https://doi.org/10.1016/j.jclepro.2020.120576.
[56] Y.H. Song, Y.R. Dai, Q. Hu, X.H. Yu, F. Qian, Effects of three kinds of organic acids on phosphorus recovery by magnesium ammonium phosphate (MAP) crystallization from synthetic swine wastewater, Chemosphere 101 (2014) 41–48, https://doi.org/10.1016/j.chemosphere.2013.11.019.
[57] A. Viani, L. Zárybnická, R. Sevcík, P. Mácová, J. Machotová, K. Veltruská, Struvite-K crystal growth inhibition by citric acid: formation of complexes in solution and surface adsorption effects, J. Cryst. Growth 598 (2022) 126858, https://doi.org/10.1016/j.jcrysgro.2022.126858.
[58] W.M. Wang, X. Xin, B. Li, H.M. Huang, X.N. Liu, L. Song, X.F. Wu, Y.F. Huang, Effect of organics on cu and cr in recovered struvite from synthetic swine wastewater, J. Clean. Prod. 360 (2022) 132186, https://doi.org/10.1016/j.jclepro.2022.132186.
[59] J.N. Yan, M.Y. Ma, F.H. Li, Phosphorus recovery via struvite crystallization in batch and fluidized-bed reactors: roles of microplastics and dissolved organic matter, J. Hazard. Mater. 476 (2024) 135108, https://doi.org/10.1016/j.jhazmat.2024.135108.
[60] Q. Li, X.C. Liu, N.N. Hou, J. Wang, Y.R. Wang, W.Q. Li, J.Q. Chen, Y. Mu, Roles of humic acid on vivianite crystallization in heterogeneous nucleation for phosphorus recovery, J. Clean. Prod. 367 (2022) 133056, https://doi.org/10.1016/j.jclepro.2022.133056.
[61] J. Pavez-Jara, W.P. Iswarani, J.B. van Lier, M.K. de Kreuk, Role of the composition of humic substances formed during thermal hydrolysis process on struvite

precipitation in reject water from anaerobic digestion, J. Water Process Eng. 59 (2024) 104932, https://doi.org/10.1016/j.jwpe.2024.104932.
[62] S. Polat, P. Sayan, Preparation, characterization and kinetic evaluation of struvite in various carboxylic acids, J. Cryst. Growth 531 (2020) 125339, https://doi.org/10.1016/j.jcrysgro.2019.125339.
[63] B.N. Song, R.H. Wang, W.Q. Li, Z.S. Zhan, J.Y. Luo, Y. Lei, Fate of micropollutants in struvite production from swine wastewater with sacrificial magnesium anode, J. Hazard. Mater. 478 (2024) 135505, https://doi.org/10.1016/j.jhazmat.2024.135505.
[64] H. Arslanoglu, F. Tumen, Potassium struvite (slow release fertilizer) and activated carbon production: resource recovery from vinasse and grape marc organic waste using thermal processing, Process Saf. Environ. Prot. 147 (2021) 1077–1087, https://doi.org/10.1016/j.psep.2021.01.025.
[65] A.M. Bennett, S. Lobanov, F.A. Koch, D.S. Mavinic, Improving potassium recovery with new solubility product values for K-struvite, J. Environ. Eng. Sci. 12 (2017) 93–103, https://doi.org/10.1680/jenes.17.00019.
[66] F. Abbona, H.E.L. Madsen, R. Boistelle, Crystallization of 2 magnesium phosphates, struvite and newberyite - effect of ph and concentration, J. Cryst. Growth 57 (1982) 6–14, https://doi.org/10.1016/0022-0248(82)90242-1.
[67] D. Crutchik, A. Sánchez, J.M. Garrido, Simulation and experimental validation of multiple phosphate precipitates in a saline industrial wastewater, Sep. Purif. Technol. 118 (2013) 81–88, https://doi.org/10.1016/j.seppur.2013.06.041.
[68] C.K. Chauhan, P.M. Vyas, M.J. Joshi, Growth and characterization of Struvite-K crystals, Cryst. Res. Technol. 46 (2011) 187–194, https://doi.org/10.1002/crat.201000587.
[69] A.T. Bah, Z.Y. Shen, J.N. Yan, F.H. Li, Phosphorous recovery from water via batch adsorption enrichment combined with struvite crystallization in a fluidized bed reactor, J. Environ. Chem. Eng. 11 (2023) 110180, https://doi.org/10.1016/j.jece.2023.110180.
[70] S. Atalay, I. Sargin, G. Arslan, Crystallization of struvite-K from pumpkin wastes, J. Sci. Food Agric. 102 (2022) 523–530, https://doi.org/10.1002/jsfa.11380.
[71] S. Graeser, W. Postl, H.P. Bojar, P. Berlepsch, T. Armbruster, T. Raber, K. Ettinger, F. Walter, Struvite-(K), $KMgPO_4{\cdot}6H_2O$, the potassium equivalent of struvite - a new mineral, Eur. J. Miner. 20 (2008) 629–633, https://doi.org/10.1127/0935-1221/2008/0020-1810.
[72] A. Vuillemin, A. Friese, R. Wirth, J.A. Schuessler, A.M. Schleicher, H. Kemnitz, A. Lücke, K.W. Bauer, S. Nomosatryo, F. von Blanckenburg, R. Simister, L. G. Ordoñez, D. Ariztegui, C. Henny, J.M. Russell, S. Bijaksana, H. Vogel, S. A. Crowe, J. Kallmeyer, T.D.P.S. Team, vivianite formation in ferruginous sediments from lake towuti, Indonesia, Biogeosciences 17 (2020) 1955–1973, https://doi.org/10.5194/bg-17-1955-2020.
[73] A. Yesigat, A. Worku, A. Mekonnen, W. Bae, G.L. Feyisa, S. Gatew, J.L. Han, W. Z. Liu, A.J. Wang, A. Guadie, Phosphorus recovery as K-struvite from a waste stream: a review of influencing factors, advantages, disadvantages and challenges, Environ. Res. 214 (2022) 114086, https://doi.org/10.1016/j.envres.2022.114086.
[74] GaussView, Version 6, Roy Dennington, Todd A. Keith, and John M. Millam, Semichem Inc., Shawnee Mission, KS, 2016.
[75] L. Paltrinieri, E. Huerta, T. Puts, W. van Baak, A.B. Verver, E.J.R. Sudholter, L.C.P. M. de Smet, Functionalized Anion-Exchange membranes facilitate electrodialysis of citrate and phosphate from model dairy wastewater, Environ. Sci. Technol. 53 (2019) 2396–2404, https://doi.org/10.1021/acs.est.8b05558.
[76] F.J. Stevenson, R.A. Olsen, A simplified representation of the chemical nature and reactions of soil humus, J. Agron. Educ. 18 (1989) 84–88, https://doi.org/10.2134/jae1989.0084.